Quantitative Treatment of Magnesium Ion Adsorption at the γ-Al_2O_3−Water Interface

Lizandra M. Zimmermann,[†] Alessandra F. Silva,[†] Michelle Medeiros,[†] Jociane Bruch,[†] Aloísio J. Souza,[†] Rene A. Nome,[‡] Haidi D. Fiedler,*[,†] and Faruk Nome[†]

Departamento de Química, Universidade Federal de Santa Catarina, National Institute of Science and Technology for Catalysis, Florianópolis, SC 88040-900, Brazil, and Instituto de Química, Universidade Estadual de Campinas, SP, 13084-824, Campinas, Brazil

Received: July 1, 2010

The adsorption isotherms of Mg^{2+} on γ-alumina follow a typical Langmuir model, characteristic of single layer adsorption, and experimental data fitting is successfully described by a two-layer electrostatic model (DLM) on discrete sites on the surface with variable charge as a function of pH. Speciation studies indicate that Mg^{2+} was the major adsorbed species and the results show how chemical composition and species distribution in clay surfaces couples to solution properties such as pH and ionic strength to regulate adsorption and desorption processes in the distribution of Mg^{2+} species between sediment and the aqueous phase. Probably the mechanism of adsorption of Mg^{2+} at the γ-alumina surface is predominantly electrostatic, with outer sphere complexation, and the Mg^{2+}-saturated γ-Al_2O_3 surface efficiently promotes hydrolysis of phosphate diesters.

I. Introduction

The interest in adsorption processes extends to many fields, including hydrology, aquatic chemistry, water, and wastewater treatment in chemical, metallurgical, and petrochemical industries.[1,2] The mineral surfaces have charge densities which depend on pH and which are counterbalanced in aqueous solutions to maintain solution electroneutrality. Thus, an electrical double layer (EDL) is generated at the sorbent/water interface and the effect of EDL formation on clay-like minerals is of fundamental importance for adsorption of different metal ions. As expected, adsorption and desorption of metal ions depends on the nature of the sorbent and on the concentration of chemical additives in solution, which can act as complexants to promote desorption or enhance adsorption of the metal ion.[3,4]

Aluminum oxide is commonly used as supporting material for the preparation of new catalysts and adsorbents due to its mechanical properties and large surface area. Surface hydroxyl groups are ionizable and different species at the surface have different reactivities and constitute the complexation sites. Divalent metals adsorbed on the surface promote development of charges which depend on pH, ionic strength, and electrolytes in solution.[5−7]

Mixed-metal oxide systems can exhibit chemical properties that differ notably from those of the corresponding single component oxides and those whose initial components differ considerably in their acid−base properties are especially interesting. MgO is unique in its basicity (Hammet constant $H = +26.0$) and forms a distinct class from such oxides as alumina, silica, etc., which are acidic, neutral, or amphoteric.[8] The interaction of Mg^{2+} with hydrous oxides of Al and aluminosilicates should generate new materials with significant basicity. Clays are ubiquitous in the natural environment, and their surface chemical properties are intrinsically important in terms of environmental molecular science and control important phenomena such as release and uptake, transport, pH buffering, water quality, and soil rheological properties.[2,4,5]

In previous work,[4,5] we have analyzed the adsorption behavior of Cr^{6+} and Cd^{2+} on clays, focusing on both adsorption isotherms and species distribution at surfaces of oxide, oxyhydroxide, and clay particles. The present work describes the interaction of Mg^{2+} with the hydrated aluminum oxide surface forming a Mg^{2+}-saturated γ-Al_2O_3 surface, which is an efficient catalyst in the hydrolysis of ethyl 2,4-dinitrophenyl phosphate (EDNPP). Here we utilize adsorption isotherms and species distribution in aqueous solution and in the molecular interface to describe the adsorption of Mg^{2+} at the γ-Al_2O_3 surface, where fitting of the experimental data is consistent with a two-layer electrostatic model (DLM).

II. Experimental Section

Instrumentation. An ionic chromatography instrument (Metrohm 761 Compact, Herisau, Switzerland) was used in adsorption experiments to quantify free Mg^{2+} and Na^+ concentrations. The column used was Metrosep C2 150, size 150/4.0 mm (order no. 6.1010.220 Metrohm) for cations. Oxalic acid (2.7 mmol dm^{-3}) has been used as eluent (flow 0.80 mL/min, temperature 20 °C, pressure 6.0 MPa and 14 min for retention time using a 20 mg dm^{-3} magnesium solution).

UV−visible spectrophotometric measurements were carried out on a FEMTO 800 XI spectrophotometer equipped with deuterium and tungsten lamps and a 1 cm quartz cell. Doubly deionized water with conductivity less than 5.6×10^{-8} Ω^{-1} cm^{-1} and pH between 6.4 and 6.8 from a NANOpure analytical deionization system (type D-4744) was used to prepare solutions of standards and reagents.

A Philips PW 2400 X-ray spectrometer (WDXRF) with Rh excitation tube (3 kW) was used to determine the components and X-ray fluorescence spectroscopy (XRF) samples were prepared as lithium tetraborate (1:10) melts. Calibration was carried out with ca. 68 series of natural geological reference materials for clay and sand minerals.

* To whom correspondence should be addressed. E-mail: fiedler@qmc.ufsc.br.
[†] Universidade Federal de Santa Catarina.
[‡] Universidade Estadual de Campinas.

10.1021/jp106094y
Published on Web 08/18/2010

TABLE 1: Chemical Compositions (%) Obtained by XRF for γ-Alumina

	SiO_2	Al_2O_3	K_2O	Fe_2O_3	CaO	Na_2O	MgO	TiO_2	P_2O_5	LOI[a]	MnO
γ-Al_2O_3	nd[b]	95.68	0.06	0.02	0.05	2.03	nd[b]	nd[b]	0.09	nd[b]	2.23

[a] LOI: loss of ignition. [b] nd: not detected.

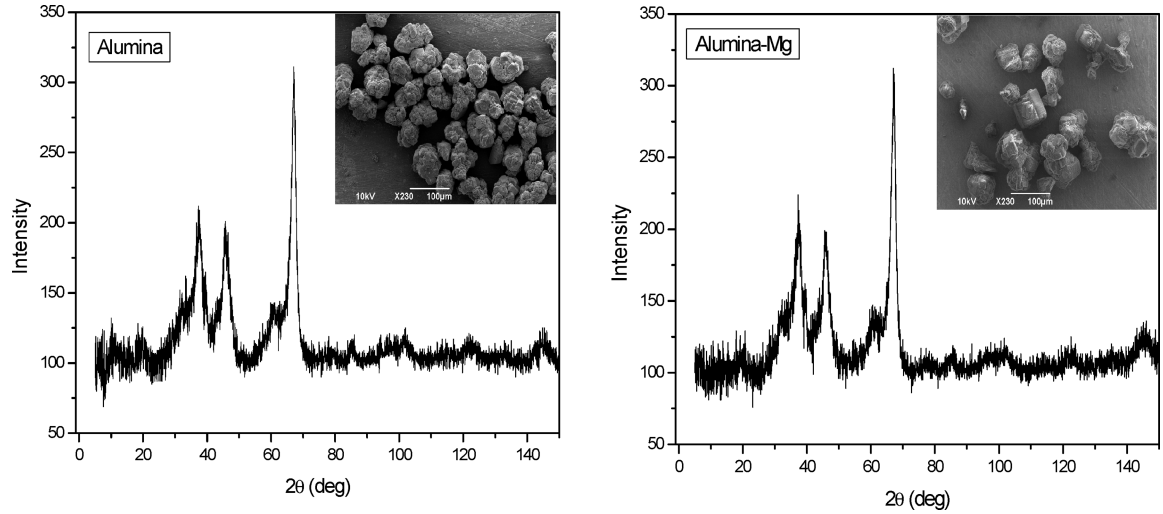

Figure 1. Micrographs of (A) γ-alumina and (B) γ-alumina$-Mg^{2+}$ and X-ray diffraction (XDR) patterns.

Adsorption Experiments. γ-Alumina (aluminum oxide 90 active basic) from Merck has the chemical composition given in Table 1, obtained by X-ray fluorescence spectroscopy analysis (XRF).

At the beginning of the adsorption experiment 20 mL of Mg^{2+} (Fluka, Steinheim, Germany), initial concentration usually from 0 (as a blank solution) to 100 mg dm^{-3}, was added to 1 g of alumina in a polypropylene tube (50 mL), and the mixture was kept at 25 °C in a Dubnoff type water bath, at a reciprocal shaking speed of 120 rpm, for 1 h. The solution was filtered through a 0.45-μm Schleicher and Schuell filter membrane and the solution was then analyzed by ionic chromatography as previously described. The amount of Mg^{2+} sorbed was calculated from the difference between initial and final free Mg^{2+} concentrations. Adsorption experiments were carried out at room temperature (23−25 °C) in the presence of ambient CO_2. Initially, under the same adsorption conditions, a kinetic experiment was carried out with 1.44 mmol dm^{-3} of total magnesium concentration to determine the time necessary for equilibrium attainment. The equilibrium for the adsorption of Mg^{2+} in γ-Al_2O_3 was reached in less than 1 h.

Micrograph of Alumina and Mg^{2+}−Alumina. Micrographs of γ-alumina powder with and without magnesium were made to observe any structural change in the physical proprieties of the γ-alumina due to magnesium adsorption. Images were made by scanning electron microscope (SEM), model JEOL JSM-6390LV, with an embedded energy dispersive X-ray analyzer (EDS).

III. Results and Discussion

Physical Structures of γ-Al_2O_3 and Mg^{2+}−γ-Al_2O_3. Micrographs of γ-alumina powder and X-ray diffraction (XRD) measurements with and without magnesium were performed to compare any change in the surface structure of the γ-alumina due to magnesium adsorption. Figure 1 shows X-ray diffraction data and scanning electron microscopic images for γ-alumina (Figure 1A) and γ-alumina$-Mg^{2+}$ (Figure 1B). The diffraction data in Figure 1A are consistent with the γ-alumina structure,[9,10] and Figure 1B displays the same essential features (peak positions and peak intensities) as in Figure 1A. Moreover, SEM images indicate similar physical appearances for both samples and the micrographs in Figure 1 show particles that continue to be γ-alumina, with Mg^{2+} on the surface not significantly affecting the crystal structure.

Quantitative Treatment of Mg^{2+}−γ-Al_2O_3 Surface Equilibria. Chemical equilibrium studies on aqueous Mg^{2+} and water/γ-alumina have been reported in great detail. However, the combined Mg^{2+}−γ-Al_2O_3 system presents new and complex equilibria and interactions, all of which are relevant to a better understanding of this system at the level of environmental molecular science. In our quantitative treatment of the Mg^{2+}−γ-Al_2O_3 system, we initially review the distribution of Mg^{2+} species in aqueous solution, and follow with analysis of titration data for γ-Al_2O_3 in water. Finally, we consider the problem of Mg^{2+} complexation at the water−γ-Al_2O_3 interface.

The distribution of different Mg^{2+} species in aqueous solution depends on pH and concentration of free Mg^{2+}. The relevant mass-law expressions for the equilibria between different Mg^{2+} species are described by eqs 1 and 2.

$$Mg^{2+} + OH^- \leftrightarrows MgOH \quad K_1 = 398.1 \tag{1}$$

$$Mg(OH)_2 \leftrightarrows Mg^{2+} + 2OH^- \quad K_2 = 6.31 \times 10^{-10} \tag{2}$$

Combining eqs 1 and 2 with the mass balance eq 3 gives appropriate equations for species distribution as a function of pH (eqs 4−6).

$$[Mg_t] = [Mg^{2+}] + [Mg(OH)] + [Mg(OH)_2] \tag{3}$$

$$[Mg(OH)] = ([Mg_t]K_1K_2[OH])/(K_1K_2[OH] + [OH]^2 + K_2) \tag{4}$$

$$[Mg^{2+}] = [Mg(OH)]/(K_1[OH]) \quad (5)$$

$$[Mg(OH)_2] = [Mg_t] - [Mg^{2+}] - [Mg(OH)] \quad (6)$$

Figure 2 shows the calculated Mg^{2+} species distribution based on eqs 4−6. At pH values below 8, Mg^{2+} is the predominant species present in solution, whereas $Mg(OH)_2$ is the predominant species at pH values above 10. In the intermediate regime (pH from 8 to 10), Mg^{2+}, $MgOH^+$, and $Mg(OH)_2$ are present in solution.

To fully understand our adsorption experiments described below, we also need to analyze the pH-dependence of the water−γ-Al_2O_3 system. Figure 3 shows titration data for the γ-Al_2O_3 surface at 25 °C in a nitrogen atmosphere, and in the presence of KCl. The data are plotted as apparent acidity coefficients as a function of the fractional ionization of the surface. Data treatment followed the extrapolation method of Davis et al.[11] based on the electrical double layer model. Basically, exponential terms are added to the mass law expressions to relate the bulk solution concentration to the concentration at some location near the electrical double layer. The terms are added to correct for electrostatic field effects on surface equilibria, and are weighting factors based on a Boltzmann distribution. The constants $pK_{a1}(int) = 8.83$ and $pK_{a2}(int) = 10.48$, are the intrinsic acidity constants obtained by extrapolation of pQ_{a1} and pQ_{a2} to zero surface charge and potential in the absence of net specific adsorption. It is important to note that under the experimental conditions of this work dissolution of γ-Al_2O_3 is negligible, since we are working at pH >3 and with low ionic strengths.

Finally, combining eqs 1 and 2 describing distribution of Mg^{2+} species in solution with those describing interaction of Mg^{2+} species with the surface (eqs 7 and 8) allows the full treatment of the adsorption phenomena.

$$\equiv SOH + Mg^{2+} \rightleftharpoons SO^-Mg^{2+} + H^+ \quad (7)$$

$$K_{int}^{Mg^{2+}} = \frac{[\equiv SO^-Mg^{2+}][H^+]}{[\equiv SOH][Mg^{2+}]} \exp[(\Psi_0 - 2\Psi_\beta)F/RT] \quad (8)$$

The components of the different equilibria involved in the adsorption of Mg^{2+} in the γ-Al_2O_3 surface as a function of bulk pH are in Table 2. In the full treatment of the adsorption experiments, we used the following: (i) intrinsic pK_a values calculated for 0.001 M KCl, (ii) values of $a = [\gamma\text{-}Al_2O_3] = 40$ g/L, (iii) surface area of 156 m^2/g, determined by BET measurements, and (iv) $Ns = 1.04 \times 10^{-2}$ mol L^{-1}, estimated from the maximum adsorption obtained in the available surface area. With these parameters, we calculated the sorption and distribution of Mg^{2+} ion species at the γ-Al_2O_3 surface, in the absence of added anions, with a two pK_a DLM model and the visual-MINTEQ simulation program.

The fits with the model described in the previous paragraph are in Table 3, where values of WSOS/DF correspond to the weighted sum of squares of residuals divided by degrees of freedom, indicating that the adjustment procedure is acceptable and some deviations are observed at lower pH values with less adsorption.

We summarize here the key points of our quantitative approach to modeling the Mg^{2+}−γ-Al_2O_3−water equilibria:

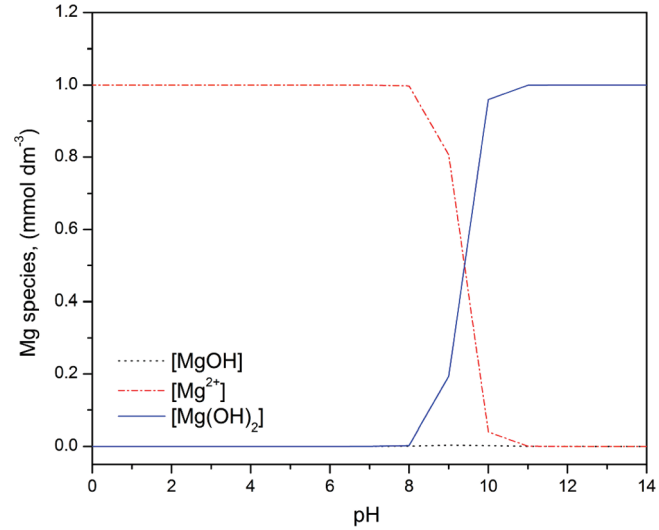

Figure 2. Species distributions for magnesium ion as a function of pH.

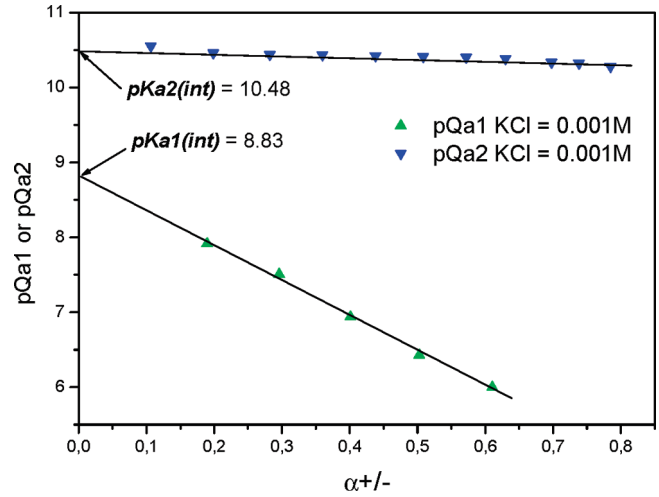

Figure 3. Apparent acidity quotient (pQ_{a1} and pQ_{a2}) as a function of the fractional ionization of the surface. Symbols α^+ and α^- represent positive and negative fractional charges, respectively.

TABLE 2: Components Used in the Intrinsic Equilibrium Expressions for the Adsorption of Mg^{2+} on γ-Alumina

species	≡SOH	$\exp(-F\Psi_0RT)^a$	$\exp(-F\Psi_\beta/RT)^b$	Mg^{2+}	H^+
H^+	1	0	0	0	1
≡SOH	1	0	0	0	1
$\equiv SO^-$	1	−1	0	0	−1
$\equiv SOH_2^+$	1	1	0	0	1
Mg^{2+}	0	0	0	1	0
$MgOH^+$	0	0	0	1	−1
$\equiv SO^-Mg^{2+}$	1	−1	2	1	−1
OH^-	0	0	0	0	−1

[a] Dummy components for accounting electrostatic effects, do not represent real chemical entities but are treated as one. [b] Dummy components for accounting electrostatic effects, do not represent real chemical entities but are treated as one.

(1) The species distribution diagram (Figure 2) of Mg^{2+} in aqueous solution is divided into three regions. Free Mg^{2+} ions in solution are the main species below pH 8.0. In the pH range 8.0−10.0, three species are present in solution: Mg^{2+}, $MgOH^+$, and $Mg(OH)_2$. Above pH 10.0, $Mg(OH)_2$ is the main species, although the low solubility product of this form complicates the analysis.

TABLE 3: Calculated Surface Complexation Constants for Mg^{2+} on γ-Al_2O_3[a]

pH	$-\log K^{int}_{Mg^{2+}}$	WSOS/DF
6.5	no convergence	
7.0	9.30	91.34
7.5	8.34	8.32
8.0	8.58	4.75
8.5	8.47	5.74
9.0	8.75	6.31
9.5	8.72	7.23

[a] a = [γ-Al_2O_3] = 40 g/L; S = 156 m^2/g; Ns = 1.04 × 10^{-2} mol·L^{-1}; pK_{a1}(int) = 10.48; pK_{a2}(int) = 8.83; C_1 = 0.8 F/m^2; C_2 = 0.2 F/m^2.

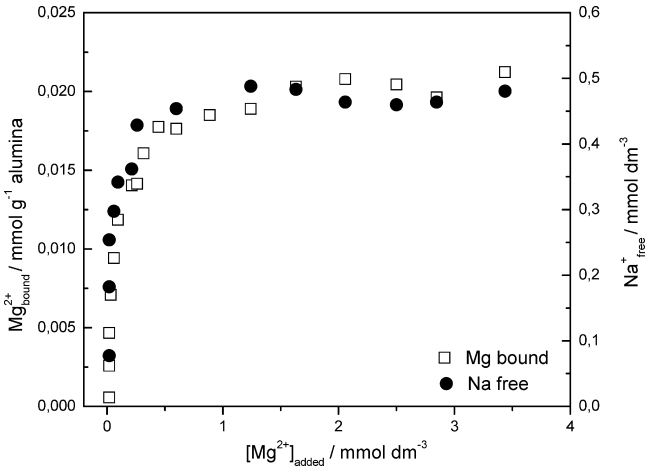

Figure 4. Relationship between magnesium added versus free sodium in solution.

(2) Titration of the γ-Al_2O_3/water system and further data analysis gave pK_{a1} = 8.83 for the most acidic group in γ-Al_2O_3. The surface acidity constant decreases significantly as the fractional surface charge, $\alpha^{+/-}$, increases (Figure 3).

(3) Equation 8 allows a quantitative treatment of Mg^{2+} adsorption at the γ-Al_2O_3/water interface. The calculations, which were parametrized with our own adsorption experimental results presented below, reveal nearly constant Mg^{2+}/γ-Al_2O_3 complexation constants in the 7.5−9.5 pH range.

Adsorption of Mg^{2+} onto γ-Al_2O_3. Adsorption experiments were carried out as described in section on Adsorption Experiments. Figure 4 shows experimental results for the amount of Mg^{2+} adsorbed onto alumina ("Mg^{2+} bound") as a function of the initial Mg^{2+} concentration in solution ("$[Mg^{2+}]_{added}$"). The amount of bound Mg^{2+} increases sharply at low initial Mg^{2+} concentrations, reaching a plateau near $[Mg^{2+}]_{added}$ = 1 mmol·dm^{-3}. The plateau value, which approximately equals 0.02 mmol of Mg^{2+} sorbed per gram of alumina, remains essentially constant as $[Mg^{2+}]_{added}$ increases up to 3.5 mmol·dm^{-3}.

Also shown in Figure 4 is the final concentration of Na^+ in solution, labeled $[Na^+]_{free}$, as a function of $[Mg^{2+}]_{added}$. In the experiments, both $[Na^+]_{free}$ and $[Mg^{2+}]_{free}$ were measured simultaneously by ionic chromatography for each value of $[Mg^+]_{added}$, so that a direct comparison can be made. Figure 4 shows that both $[Mg^{2+}]_{bound}$ and $[Na^+]_{free}$ follow the same trend as a function of $[Mg^{2+}]_{added}$, that is, there is ionic exchange between Mg^{2+} and Na^+ at the γ-Al_2O_3 surface. A stoichiometric exchange between Mg^{2+} and Na^+ is not expected due to the complexation reaction described by eq 8, and the scales used in Figure 4 were chosen to emphasize the qualitative trend mentioned above. The important point here is that the ionic exchange between Mg^{2+} and Na^+ illustrates the complexity of the multicomponent equilibria associated with Mg^{2+} adsorption at the γ-Al_2O_3/water interface.

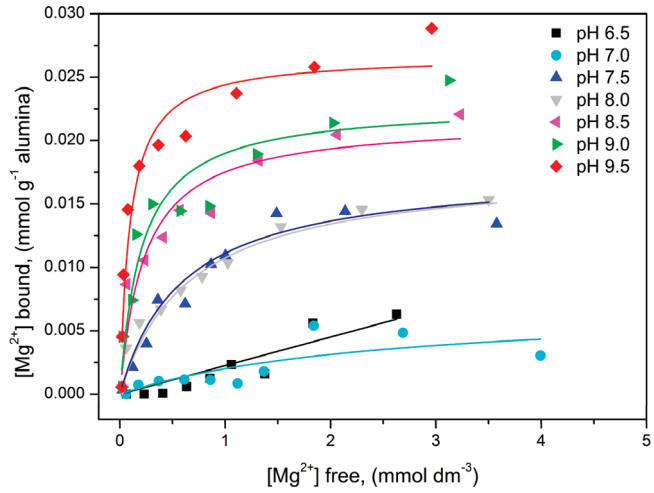

Figure 5. Mg^{2+} adsorption isotherms in γ-Al_2O_3 as a function of pH, at 25 °C, equilibrium time = 60 min. Symbols given in the figure denote pH values at which the experimental data was obtained.

The equilibrium for the adsorption process of Mg^{2+} on γ-Al_2O_3 was reached in less than 1 h. The adsorption data are typical of a Langmuir isotherm and the sorption of Mg^{2+} is accompanied by desorption of sodium ion. Clearly, the use of ion chromatography for the simultaneous quantification of magnesium and sodium ions allows characterization of a typical ion-exchange reaction at the alumina surface, with the sorption of Mg^{2+} exchanging and desorbing Na^+. It is important to note that experimentally, a sodium peak appeared in the chromatogram in the blank solution (consistent with the presence of sodium in the basic alumina) and this peak increases upon addition and sorption of Mg^{2+} onto the alumina surface (not shown). When the surface is saturated with Mg^{2+}, there is no further liberation of Na^+ in solution.

Adsorption of Mg^{2+} onto γ-Al_2O_3: pH Dependence. The pH-dependence of Mg^{2+} adsorption onto γ-Al_2O_3 was studied at 25.0 °C at pH range 6.5−9.5 (Figure 5). The amount of Mg^{2+} bound to γ-Al_2O_3 is clearly pH-dependent. At pH values of 6.5 and 7.0, the amount of $[Mg]_{bound}$ is relatively small for any given $[Mg]_{added}$. In the pH range from 7.5 to 9.5, an increase in bound Mg^{2+} is observed with increasing pH; this trend is clearly seen at low $[Mg]_{added}$. Moreover, as $[Mg]_{added}$ increases, the amount of bound Mg^{2+} reaches a plateau in the experiments performed at pH 7.5 and 8.0, whereas at pH >8.0 $[Mg]_{bound}$ continues to increase with increasing $[Mg]_{added}$.

The adsorption data of Mg^{2+} at 25.0 °C in γ-Al_2O_3 as a function of pH shown in Figure 5 were fitted with the Langmuir isotherm (eq 9).

$$n = \frac{K_L[Mg^{2+}]M}{1 + K_L[Mg^{2+}]} \tag{9}$$

In eq 9, n corresponds to the amount adsorbed per gram of clay (mmol/g clay); K_L corresponds to the adsorption equilibrium constant; M represents the maximum adsorption (mmol/g clay),[12] and the magnesium concentrations correspond to the equilibrium solution concentration of free Mg^{2+}. The solid lines in Figure 5 were calculated with a nonlinear least-squares program, and calculated values for the different experiments are given in Table

TABLE 4: Langmuir Isotherm Parameters for Adsorption of Mg^{2+} onto γ-Al_2O_3

pH	M (mmol g^{-1})	K_L (L $mmol^{-1}$)
6.5	0.002	
7.0	0.007	15.9
7.5	0.018	58.8
8.0	0.018	66.7
8.5	0.024	166
9.0	0.024	200
9.5	0.027	500

4. As expected, both the value of the Langmuir constant K_L and of the maximum capacity (M) increase with pH.

It is important to note that, while the Langmuir isotherm fitted adequately all of the data, especially at pH 7.5 and 8.0, the concentration of free Mg^{2+} needed to saturate the γ-Al_2O_3 surface is rather high when compared to environmental conditions in river water, but not in oceans (typically in the range of 3−20 mg/L in rivers and an average of 1350 mg/L in seawater). This result indicates that in most conditions in natural waters the distribution of Mg^{2+} between the different geochemical phases of the sediment follows a simple linear relationship.[13−18]

The species distribution calculation (Figure 2) is useful in understanding our adsorption experiments (Figure 5) and the Langmuir parameters in Table 4. Thus, the observed increases in binding and affinity of Mg^{2+} with the γ-Al_2O_3 surface as the pH increases occur mainly in the region where Mg^{2+} is the predominant species in solution, that is, at or below pH 8. On the other hand, at pH >9 there is significant formation of $Mg(OH)_2$, which is in equilibrium with MgO and precipitates. Therefore, above pH 9−9.5 precipitation of $Mg(OH)_2$/MgO complicates a quantitative study of the sorption process.

The very nature of a Langmuir-type treatment gives little information about the microscopic constants involved in the adsorption process. However, the experimental results in Figure 5 and the Langmuir parameters from Table 4 highlight the importance of pH for adsorption of Mg^{2+} on γ-alumina. In addition to controlling the species distribution of Mg^{2+}, the solution pH also affects the surface chemical properties. Given the amphoteric character of γ-alumina, the species distribution at the surface depends upon protonation equilibria and therefore on pH. For example, we found it difficult to promote magnesium adsorption on γ-alumina at low pH (below pH 7.0), consistent with the amphoteric behavior of the surface, where charge is strongly pH dependent, becoming positive at low pH. Therefore, the pH dependence of the Langmuir parameters shown in Table 4 is strongly indicative that surface charge plays a predominant role in the sorption of Mg^{2+}.

By using the calculated surface complexation constants for Mg^{2+} on γ-Al_2O_3 in Table 3, we fitted the experimental adsorption data at various pH values. The solid lines in Figure 5 are in good agreement with experimental data, especially at pH 8.5−9.5 where adsorption is significant. Therefore the results in Figure 6 show that the proposed model is consistent with the adsorption data, allowing calculation of $-\log K^{INT}_{Mg^{2+}_{out}} = 8.57 \pm 0.17$.

The calculated equilibrium constants are clearly indicative that free Mg^{2+} ion plays a dominant role and is responsible for practically all adsorbed Mg^{2+} on the γ-Al_2O_3 surface. Furthermore, the $\equiv SO^-$ sites of alumina are of paramount importance and contributions of the neutral ($\equiv SOH$) and positively charged ($\equiv SOH_2^+$) species at the alumina surface are less important for sorption of Mg^{2+}.

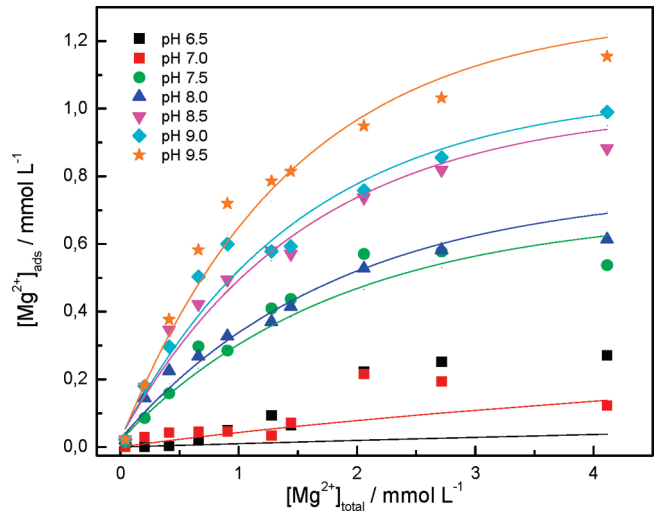

Figure 6. Mg^{2+} adsorption isotherms measured at 25 °C for γ-Al_2O_3 as a function of pH. Solids line calculated with FITEQL as described in the text.

Hydrolysis of Ethyl 2,4-Dinitrophenyl Phosphate (EDNPP). The catalytic efficiency of the Mg^{2+}-covered γ-Al_2O_3 was tested in aqueous solutions on the hydrolysis of EDNPP, which was chosen as the organic reagent because under some conditions phosphodiesters are the least reactive esters of phosphoric acid.[19,20] The reaction of EDNPP with nucleophiles is well-known and forms 2,4-dinitrophenoxide and ethylphosphate (or the corresponding derivative) and can be conveniently analyzed by monitoring the appearance of 2,4-dinitrophenolate, eq 10.

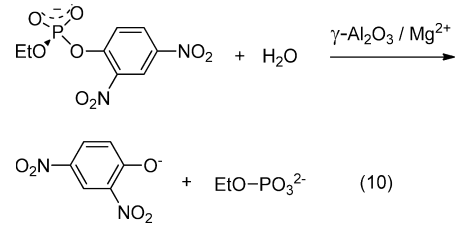

(10)

The hydrolysis of EDNPP in the presence of Mg^{2+}-covered γ-Al_2O_3, proceeds with a rate constant of 1.2×10^{-3} s^{-1}, which is 4-fold faster than hydrolysis of EDNPP in a 1.0 M solution of sodium hydroxide, with a second order rate constant, $k_2 = 2.57 \pm 0.11 \times 10^{-4}$ M^{-1} s^{-1}. The results are promising and detailed studies of a variety of phosphoric acid esters are being examined in detail.

IV. Conclusions

The kinetics and equilibria of Mg^{2+} adsorption onto alumina were studied and the results analyzed in the light of surface charge densities, chemical composition, and pH. Specifically, we have experimental results and equilibrium calculations for the Mg^{2+}/γ-Al_2O_3/water system in the pH range from 6.5 to 9.5. Our main conclusion is that the complex adsorption equilibria in this system can be treated adequately with a Langmuir model, characteristic of single layer adsorption, and fitting of the experimental data is consistent with a two-pK_a double layer model (DLM Model), with Mg^{2+} ion as the major adsorbed species. The mechanism of adsorption of Mg^{2+} at the γ-alumina surface is predominantly electrostatic with outer sphere complex formation and exchange with sodium ion. We

expect these findings to be useful for understanding other complex systems with multiple equilibria, since our model assumptions sufficed to fit all the experimental results.

In a previous study, we found that chromate anion interacts strongly with clay-like minerals containing a high fraction of positively charged sites and/or at lower pH are thermodynamically more likely to be driven toward the adsorbed phase.[5] Our present results for Mg^{2+} sorption at the alumina/water interface are consistent with our previous findings, indicating that positive charges in the surface preferentially attract anions, while negatively charged surfaces promote cation adsorption. That is, the binding affinity of Mg^{2+} on γ-alumina increases as pH increases. As pH increases, there is an increase in negative charge density at the surface as well as an increase of divalent Mg^{2+} species in solution. The present investigation shows how the species distribution in alumina surfaces couples to solution properties such as pH to regulate the adsorption and desorption processes and the highly basic Mg^{2+}-saturated γ-Al_2O_3 surface acts as an efficient catalyst in the hydrolysis of ethyl 2,4-dinitrophenyl phosphate (EDNPP).

Finally, we speculate on the adsorption of Mg^{2+} onto various surfaces. We expect very little Mg^{2+} sorption onto minerals with a larger fraction of silica and a smaller fraction of alumina, especially at neutral or acidic pH.

Acknowledgment. The authors thank PRONEX, CNPq, FAPESC, and Capes for financial support, Profs. Hugo Gallardo and Ivan Bertold for X-ray diffraction (XRD) measurements, Marlon Beninca for initial adsorption experiments, and Deise R. Consoni for the scanning electron microscopy experiments.

References and Notes

(1) Musorrafiti, M. J.; Konek, C. T.; Hayes, P. L.; Geiger, F. M. *J. Phys. Chem. C* **2008**, *112*, 2032.

(2) Li, J.-G.; Ikegami, T.; Lee, J.-H.; Mori, T.; Yajima, Y. *J. Eur. Ceram. Soc.* **2001**, *21*, 139.

(3) Stumm, W.; Morgan, J. J.; *Aquatic Chemistry*, 3rd ed.; Wiley-Interscience: New York, 1996.

(4) Westrup, J. L.; Fritzen, M. B.; Souza, A. J.; Bedendo, G. C.; Nome, F.; Fiedler, H. D. *J. Braz. Chem. Soc.* **2005**, *16*, 982.

(5) Fritzen, M. B.; Souza, A. J.; Silva, T. A. G.; Souza, L.; Nome, R. A.; Fiedler, H. D.; Nome, F. *J. Colloid Interface Sci.* **2006**, *296*, 465.

(6) Priebe, J. P.; Satnami, M. L.; Tondo, D. W.; Souza, B. S.; Priebe, J. M.; Micke, G. A.; Costa, A. C. O.; Fiedler, H. D.; Bunton, C. A.; Nome, F. *J. Phys. Chem. B* **2008**, *112*, 14373.

(7) Boumaza, A.; Favaro, L.; Lédion, J.; Sattonnay, G.; Brubach, J. B.; Berthet, P.; Huntz, A. M.; Roy, P.; Tétot, R. J. *J. Solid State Chem.* **2009**, *182*, 1171.

(8) Kirszensztejn, P.; Przekop, R.; Szymkowiak, A.; Mackowska, E.; Gaca, J. *Microporous Mesoporous Mater.* **2006**, *89*, 150.

(9) Yang, R.; Li, X.; Wu, J.; Zhang, X.; Zhang, Z. *J. Phys. Chem. C* **2009**, *113*, 17787.

(10) Zhang, L.; Zhu, Y. J. *J. Phys. Chem. C* **2008**, *112*, 16764.

(11) Davis, J. A.; Kent, D. B. *Rev. Mineral.* **1990**, *23*, 177.

(12) Kinniburgh, D. G. *Environ. Sci. Technol.* **1986**, *20*, 895.

(13) Fiedler, H. D.; López-Sánchez, J. F.; Quevauviller, Ph.; Ure, A. M.; Muntau, H.; Rubio, R.; Rauret, G. *Analyst* **1994**, *119*, 1109.

(14) Nome, R. A.; Martinez, C. M.; Nome, F.; Fiedler, H. D. *Environ. Toxicol. Chem.* **2001**, *20*, 693.

(15) Curtius, A. J.; Seibert, E. L.; Fiedler, H. D.; Ferreira, J. F.; Vieira, P. H. F. *Quím. Nova* **2003**, *26*, 44 (abstract in English).

(16) Reeve, R. N. *Environmental Analysis*; J. Wiley & Sons: London, U.K., 1994.

(17) Drever, J. I. *The Geochemistry of Natural Waters: Surface and Groundwater Environments*, 3rd ed.; Prentice Hall: Englewood Cliffs, NJ, 1997.

(18) Hem, J. D. *Study and Interpretation of the Chemical Characteristics of Natural Water*, 3rd ed.; Departament of the Interior, U.S. Geological Survey: Alexandria, VA, 1985; Water-Supply Paper 2254.

(19) Orth, E. S.; Brandao, T. A. S.; Milagre, H. M. S.; Eberlin, M. N.; Nome, F. *J. Am. Chem. Soc.* **2008**, *130*, 2436–2437.

(20) Orth, E. S.; da Silva, P. L. F.; Mello, R. S.; Bunton, C. A.; Milagre, H. M. S.; Eberlin, M. N.; Fiedler, H. D.; Nome, F. *J. Org. Chem.* **2009**, *74*, 5011–5016.

JP106094Y